Electrochimica Acta 56 (2011) 10295–10305

Contents lists available at ScienceDirect

Electrochimica Acta

journal homepage: www.elsevier.com/locate/electacta

Interfacial electrochemistry and electrodeposition from some ionic liquids: *In situ* scanning tunneling microscopy, plasma electrochemistry, selenium and macroporous materials

Alsayed Abdel Aal[a,1], Rihab Al-Salman[a,1], Mohammad Al-Zoubi[a,1], Natalia Borissenko[a,b,1], Frank Endres[a,b,*,1], Oliver Höfft[a,1], Alexandra Prowald[a,b,1], Sherif Zein El Abedin[a,b,c,1]

[a] *Institute of Particle Technology, Clausthal University of Technology, Arnold-Sommerfeld-Strasse 6, 38678 Clausthal-Zellerfeld, Germany*
[b] *EFZN Goslar, Am Stollen 19, 38640 Goslar, Germany*
[c] *Electrochemistry and Corrosion Laboratory, National Research Centre, Dokki, Cairo, Egypt*

ARTICLE INFO

Article history:
Received 26 November 2010
Received in revised form 14 February 2011
Accepted 16 February 2011
Available online 23 February 2011

Keywords:
Ionic liquids
Herringbone reconstruction
Macroporous materials
Selenium
Electrodeposition

ABSTRACT

In this paper we report on recent results from our group, namely on the interface ionic liquid/electrode, plasma electrochemistry and electrodeposition of selenium and of macroporous structures. Ionic liquids show an interesting and liquid dependent surface chemistry: in some liquids the long range "herringbone" superstructure of Au(1 1 1) is visible, in others it is not. Glow discharge plasmas can be employed as a contact free electrode to make nanoparticles in solutions, e.g. nanoparticles of germanium. Selenium can be electrodeposited from ionic liquids under environmental conditions in an open cell and both the red and the grey phases of selenium are feasible. With the help of self organized opal structures of polystyrene spheres macroporous materials of Ag, Al and conducting polymers can be made. The prospects and limits of ionic liquids in surface electrochemistry and electrodeposition are shortly discussed.

1. Introduction

The development of air and water stable ionic liquids that can – in principle – be handled under air made ionic liquids available for a wide community and in the beginning they mainly attracted the interest of electrochemists due to their wide electrochemical windows of between 4 and 6 V. From the thermodynamic point of view the electrochemical windows should be wide enough for the electrodeposition of all metals, however, kinetic phenomena make this aim tough. For example, there are several papers where the electrodeposition of magnesium [1,2] and of titanium [3] has been reported. Mg deposition is accompanied by IL decomposition [4] and instead of elemental titanium rather non-stoichiometric titanium halides are obtained [5] and maybe ultrathin Ti layers. The electrodeposition of tantalum is quite complicated and shows a strong dependence on the liquid and the electrochemical parameters [6]. The kinetics of metal and semiconductor deposition also seem to depend on the structure and on the dynamics of the interfacial layer between the ionic liquid and the electrode surface. In [7] we have discussed how interfacial layers might influence electrochemical processes. The electrochemical double layer of ionic liquids is rather complicated and from theoretical considerations [8] it can be concluded that it rather consists of multilayers. The existence of up to 7 interfacial layers has been shown by Atkin and Warr [9] with an AFM. The interface ionic liquid/electrode has so far not yet been extensively studied, and apart from us only 2 further groups had/have activities in this field. Freyland et al. have published several papers on the initial stages of metal deposition in $AlCl_3$ based ionic liquids [10] and there are hints that in this liquid the surface of Au(1 1 1) can be probed with atomic resolution [11]. Mao et al. have concentrated on liquids with the BF_4^- anion. They have hints that this anion is specifically adsorbed on single crystalline gold surfaces, furthermore the imidazolium cations seem to be adsorbed in an ordered manner on the electrode surface [12]. An uncertainty in all surface studies with ionic liquids is their purity: ionic liquids can contain halide and Li^+ impurities in the several hundred ppm regime if made by a metathesis reaction. The BF_4^- is subject to decomposition in the presence of water and "purification" with adsorbents can introduce impurities into the liquids [13]. Thus it is of eminent importance to have a detailed

* Corresponding author at: Institute of Particle Technology, Clausthal University of Technology, Arnold-Sommerfeld-Strasse 6, 38678 Clausthal-Zellerfeld, Germany. Tel.: +49 5323 72 3141; fax: +49 5323722460.
E-mail address: frank.endres@tu-clausthal.de (F. Endres).
[1] All authors have equally contributed to this paper and are listed in alphabetic order.

0013-4686/$ – see front matter © 2011 Elsevier Ltd. All rights reserved.
doi:10.1016/j.electacta.2011.02.063

understanding of the liquid's quality if fundamental studies are performed. After more than 10 years of experience we employ meanwhile for fundamental studies solely custom-made liquids with a defined purity protocol where all impurities are guaranteed to be below 10 ppm. A few years ago we applied for the first time a glow discharge plasma as a contact free electrode for the deposition of silver nanoparticles [14] in a room temperature ionic liquid. Due to the extremely low vapour pressure of ionic liquids stable plasmas are obtained which allow a systematic study of the fundamental processes. Subsequently this method was also applied by other groups [15,16] and the method has the potential for the large scale production of reactive metal or semiconductor nanoparticles. Ionic liquids are also suited to the deposition of selenium, e.g. for CIS (copper indium selenide) solar cells. We could show that the grey phase of Se can be made from $SeCl_4$ in an ionic liquid under the conditions of an inert gas [17]. Selenium can be deposited in aqueous solutions [18,19], but for a technical process the current densities are not high enough. Selenium deposition from ionic liquids under environmental conditions could be interesting. ILs influence the morphology and increasing of the temperature over the 100 °C limit of water makes it possible to get exclusively the grey phase of selenium. Macroporous materials, especially 3DOM (3 dimensional ordered macroporous) photonic crystals, can also be electrodeposited from ionic liquids. The usually low surface tension of ionic liquids allows a penetration of the liquid through the opal structure to the electrode surface and it could be shown that photonic crystals of germanium with a photonic band gap [20,21] and macroporous Al as a possible anode host material in lithium (ion) batteries [22] can be made.

In the present paper we show that the IL/electrode interface is quite complicated. In 1-butyl-1-methylpyrrolidinium tris(pentafluoroethyl)trifluorophosphate ([$Py_{1,4}$]FAP) the herringbone superstructure of Au(1 1 1) is visible, but not in 1-ethyl-3-methylimidazolium tris(pentafluoroethyl)trifluorophosphate ([EMIm]FAP) under the same experimental conditions. Germanium nanoparticles can be made by plasma electrochemistry in 1-ethyl-3-methylimidazolium bis(trifluoromethylsulfonyl)amide ([EMIm]TFSA) from a Ge(II)–dioxane complex. Selenium can be deposited under environmental conditions and via a polystyrene sphere template assisted method macroporous materials are accessible.

2. Experimental

1-butyl-1-methylpyrrolidinium tris(pentafluoroethyl)trifluorophosphate ([$Py_{1,4}$]FAP) and 1-ethyl-3-methylimidazolium tris(pentafluoroethyl)trifluorophosphate ([EMIm]FAP) were purchased from MERCK in the highest available quality. The liquids were custom-made and the purity protocols delivered by Merck showed that all detectable impurities were below 10 ppm. There were no hints for HF or oxides. 1-ethyl-3-methylimidazolium bis(trifluoromethylsulfonyl)amide ([EMIm]TFSA), 1-butyl-1-methylpyrrolidinium trifluoromethylsulfonate ([$Py_{1,4}$]TFO) and 1-ethyl-3-methylimidazolium trifluoromethylsulfonate ([EMIm]TFO) were purchased from IOLITEC. All detectable impurities were below 40 ppm. As a rule all newly delivered ionic liquids are analyzed in our laboratory by cyclic voltammetry, XPS and *in situ* STM to ensure the purity. Prior to use, the liquids were dried under vacuum at 100 °C to water contents well below 10 ppm and stored in a closed bottle in an argon-filled glove box with water and oxygen contents below 2 ppm (OMNI-LAB from Vacuum-Atmospheres). *In situ* STM measurements were performed with Au(1 1 1) (a 300 nm thick film on mica) purchased from Agilent. Directly before use the substrates were carefully heated in a hydrogen flame to minimize possible surface contaminations. Cyclic voltammetry measurements were carried out in the glove box using a Parstat 2263 potentiostat/galvanostat (Princeton Applied Research) controlled by a PowerCV software. The electrochemical cell was made of polytetrafluoroethylene (Teflon) and clamped over a Teflon-covered Viton O-ring onto the substrate, thus yielding a geometric surface area of the working electrode of 0.3 cm^2. Platinum wires (Alfa Aesar, 99.99%) of 0.5 mm diameter were applied as quasi-reference (RE) and counter (CE) electrodes, respectively. Although not perfect with respect to stability this quasi reference electrode excludes any contamination, especially for *in situ* STM experiments. The STM-experiments were performed at room temperature using in-house-built STM heads and scanners under inert gas conditions (H_2O and O_2 <2 ppm) with a Molecular Imaging PicoScan 2500 STM controller in feedback mode. Assembling of the STM head and filling of the electrochemical cell were performed in an argon-filled glove box solely reserved for assembling of STM heads. The STM head was placed inside an argon-filled vacuum-tight stainless steel vessel, to ensure inert gas atmosphere during the STM experiments, transferred to the air-conditioned laboratory ($T = 23 \pm 1$ °C) and placed onto a vibration damped table from IDE (Germany). STM tips were made by electrochemical etching of Pt–Ir wires (90/10, 0.25 mm diameter) with a 4 mol/L NaCN solution and subsequently electrophoretically coated with an electropaint (BASF ZQ 84-3225 0201). During the STM experiments the potential of the working electrode was controlled by the PicoStat from Molecular Imaging. For our plasma investigations we have dissolved 0.1 mol/L of the $GeCl_2$·dioxane complex in [EMIm]TFSA. The setup for the particle production consists of a DC plasma reactor with a controlled argon atmosphere inside an inert gas glove box (OMNI-LAB from Vacuum-Atmospheres). Details of the whole setup can be found in [23]. 2–3 mL of the solution was put in the glass cell and carefully out-gassed at 0.1 Pa. Then the plasma was ignited at a pressure of 100 Pa at a current of 10 mA. In our experiments the electrode above the liquid acted as a cathode and the other one as an anode. Thus, electrons are accelerated to the surface of the ionic liquid. After ignition the voltage drops rapidly from 1000 V to 450–500 V. After the reaction the particles were analyzed by transmission electron microscopy. The electrochemical experiments on the electrodeposition of selenium were carried out under open air conditions, using a three-electrode cell setup. Water was added to the liquids for the deposition of selenium. For the macroporous materials polystyrene (PS) spheres with diameters of 581 nm or 600 nm (Duke Scientific) were suspended in pure ethanol (10 vol% PS in ethanol). The substrates (aluminium, gold, or indium tin oxide (ITO) coated glass) were cleaned directly before use. The aluminium foil was washed in acetone and ethanol, Au(1 1 1) was carefully heated in a hydrogen flame. ITO glass substrates were rinsed under sonication in limonene and dried in a drying cabinet. After deposition of a polystyrene opal structure these template electrodes were employed for the electrodeposition experiments.

3. Results and discussion

3.1. In situ STM measurements: the herringbone superstructure

We have been interested in the interface electrode/ionic liquid for more than 10 years now and we observed that several parameters affect the quality of an *in situ* STM experiment. One major aspect is the purity of the liquids, but we also observed that there are time dependent effects which can change the results within just one cyclic voltammetry cycle. In this paper we present *in situ* STM results on the interface Au(1 1 1) with 2 liquids, namely [$Py_{1,4}$]FAP and [EMIm]FAP. Naively one might expect that the different cation does not play a role, effectively there is a great difference between both liquids at the interface.

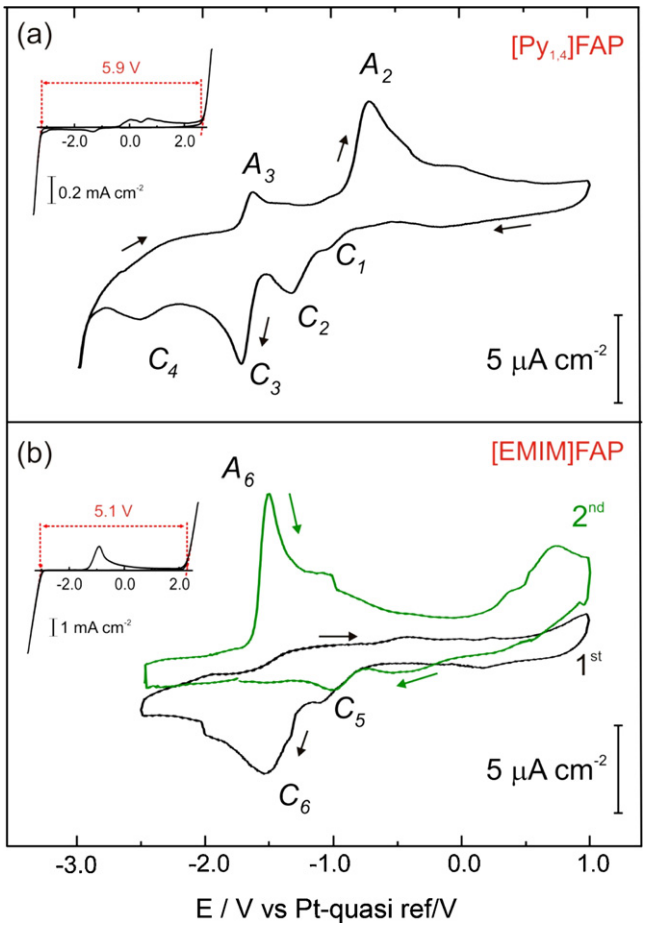

Fig. 1. Cyclic voltammograms of $[Py_{1,4}]$FAP (a) and [EMIm]FAP (b) ionic liquids on Au(1 1 1) at 25 °C at the scan rate of 10 mV/s.

Fig. 1 represents the typical cyclic voltammograms of the custom-made $[Py_{1,4}]$FAP and [EMIm]FAP ionic liquids on Au(1 1 1) at 25 °C, respectively. Scans were initially swept cathodically from the open circuit potential with a scan rate of 10 mV/s. The electrochemical windows were determined by extrapolation of the rising cathodic and rising anodic currents to zero. $[Py_{1,4}]$FAP/Au(1 1 1) exhibits a stability regime of about 5.9 V (inset in Fig. 1a) limited by gold oxidation and at the cathodic limit by the irreversible reduction of the organic cation. The broad oxidation process from 0 V to +1.5 V is correlated with the oxidation of the reduction product of the cation as this process does not appear if the scan is reversed at −3.0 V. This cyclic voltammogram looks quite perfect, however, by zooming in the potential range between −3.0 V and +1.0 V at least 4 cathodic processes (C_1–C_4) can be identified (Fig. 1a). The C_1–C_3 cathodic waves are attributed to different surface processes that occur upon IL adsorption and can be probed by *in situ* STM. The broad process C_4, that sets in prior to the decomposition of the $[Py_{1,4}]^+$ is likely correlated with the partial reduction of the organic cation. The oxidation peaks A_2 and A_3 are directly correlated with the cathodic processes C_2 and C_3 as these anodic waves appear once the scanning potentials reach that required for C_2 and C_3. The electrochemical window of [EMIm]FAP is about 5.1 V limited by the cathodic breakdown of $[EMIm]^+$ and gold oxidation (inset in Fig. 1b). The broad anodic wave in the reverse scan is mainly associated with the oxidation of the cathodic breakdown products of $[EMIm]^+$ because it is only obtained when the scanning potential exceeds the cathodic decomposition potential. By zooming in the potential range between −2.5 V and +1.0 V at least 2 cathodic processes (C_5 and C_6) can be obtained (Fig. 1b, 1st scan). Interestingly the second scan shows a surprisingly different behavior as now a huge anodic process A_6 is obtained while the cathodic process C_6 seems to disappear. (Fig. 1b, 2nd scan). This behavior remains invariable by subsequent scanning. As in both liquids all impurities are guaranteed by Merck to be below 10 ppm and as all parts in contact with the liquid were purified with H_2O_2/H_2SO_4 before, it is unlikely that these alterations and the peaks in the voltammograms are due to impurities like, e.g. halide or water. An uncertainty will always remain as even under the conditions of an inertgas glove box water traces might be absorbed by the liquid.

Fig. 2 shows *in situ* STM images of the Au(1 1 1) surface under $[Py_{1,4}]$FAP at different electrode potentials. At the ocp (−0.2 V) the typical Au(1 1 1) surface characterized by large flat terraces separated by steps of about 250 pm in height is obtained (Fig. 2a). However by decreasing the electrode potential a surface reconstruction appears and at −1.2 V the gold surface is completely reconstructed and the terraces exhibit a long-range ("herringbone") superstructure pattern (Fig. 2b). The reconstruction of Au(1 1 1) is well known and has been thoroughly investigated in vacuum using STM technique [24–28]. Quite a similar reconstruction has been found for gold electrodes in aqueous solutions [29–33]. It was reported that the electrode potential applied to the surface may lead to a surface reconstruction. Furthermore, the specific adsorption of anions may lift the reconstruction [32]. However, the $(22 \times \sqrt{3})$ reconstruction of Au(1 1 1) has not yet been reported for ionic liquids. Interestingly, by further reducing of the electrode potential, the Au(1 1 1) surface changes again and at −2.0 V we get the typical flat terraces of Au(1 1 1), Fig. 2c. In contrast, Au(1 1 1) in [EMIm]FAP is – surprisingly – not subject to such a strong surface restructuring (Fig. 3). At the open circuit potential the Au(1 1 1) terraces can be identified (Fig. 3a). When the electrode potential is reduced to −1.2 V the Au(1 1 1) surface does not exhibit the $(22 \times \sqrt{3})$ reconstruction (Fig. 3b) and at −2.0 V the gold terraces are not obtained (Fig. 3c). We should mention the following surprising effect: during the 1st STM scan in [EMIm]FAP a layer starts to grow at −1.7 V and then the surface only slowly changes. This might be due to the adsorption of the organic cation. If the electrode potential is subsequently set back to ocp and then set to values between −1.5 and −2.0 V the layer looks different (Fig. 3d–f). Although we cannot give a satisfactory explanation at the moment why [EMIm]FAP behaves so much different than $[Py_{1,4}]$FAP, we would like to raise the attention of the reader that there might be very slow processes at the interface electrode/ionic liquid. The differences in surface morphology as a function of the potential can be attributed to the specific interaction of the IL species with the gold surface. In previous studies we found that Au(1 1 1) in ultra pure $[Py_{1,4}]$TFSA ionic liquid shows a herringbone like reconstruction upon application of a negative electrode potential (−1.6 V) [34]. In contrast, when [EMIm]TFSA is employed, the Au(1 1 1) surface does not show the herringbone structure under the same experimental conditions [35]. With [EMIm]FAP we have also not yet seen the herringbone structure. Thus, when ionic liquids with pyrrolidinium cation ($[Py_{1,4}]$TFSA, $[Py_{1,4}]$FAP) are applied, the Au(1 1 1) surface undergoes $(22 \times \sqrt{3})$ reconstruction while in the case of imidazolium-based ionic liquids the herringbone reconstruction is not obtained or at least not seen.

3.2. Plasma electrochemistry: germanium nanoparticles

The plasma-electrochemical approach is hitherto the only electrochemical route to the synthesis of free nanoparticles. The question is now, if it is possible to use the plasma approach to directly synthesize semiconductor nanoparticles in ionic liquids. Semiconductor nanoparticles have interesting properties like for example a size dependent band gap. From earlier studies we know, that nanoscale silicon and germanium films can be

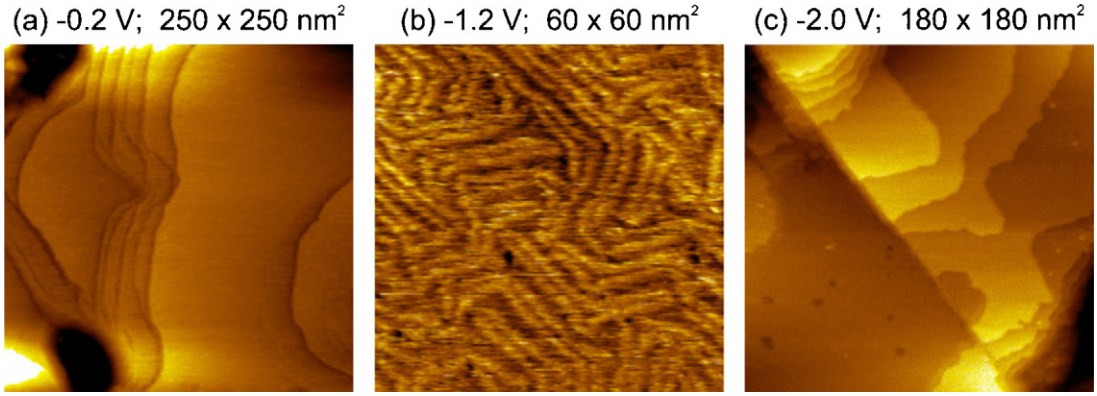

Fig. 2. *In situ* STM images of Au(1 1 1) surface in $[Py_{1,4}]$FAP at different electrode potentials.

electrodeposited from different ionic liquids with $SiCl_4$ and $GeCl_4$ as precursors [34,36]. However, due to the high vapour pressures of these common semiconductor compounds most of the dissolved precursor is pumped out of the liquid during the outgassing and the following plasma process. To overcome this problem we used a $GeCl_2$·dioxane complex ($GeCl_2C_4H_8O_2$) as a precursor for our plasma experiments, which is a solid material at room temperature. For the plasma experiment we dissolved 0.1 mol/L of the $GeCl_2$·dioxane complex in [EMIm]TFSA. Before the experiments, the solution/suspension was characterized with cyclic voltammetry (CV). The CV of the liquid with the complex shows that it is easy to electrodeposit germanium from such solutions/suspensions. 2–3 mL of the solution was put in the glass cell and carefully outgassed at 0.1 Pa. Then the plasma was ignited at a pressure of 100 Pa at a current of 10 mA. In our experiments the electrode above the liquid acted as a cathode and the other one as an anode. Thus, electrons are accelerated to the surface of the ionic liquid. After ignition the voltage drops rapidly from 1000 V to 450–500 V. In Fig. 4a the plasma experiment for $GeCl_2$·dioxane-[EMIm]TFSA solution is shown. The upper left image shows the pure 0.1 M solution/suspension. It is clearly visible that during plasma interaction (ca. 30 min) the liquid changes from milky to an orange coloured liquid, finally it turns red. The colourization starts at the plasma ionic liquid interface and is not due to the slight increase in temperature. In the lower figure the corresponding TEM measurement is shown. For these measurements a small drop of the ionic liquid with the produced nanoparticles was placed onto a TEM grid after 30 min of plasma exposure. Particles with a size below 50 nm are observable (see Fig. 4b). A similar colour effect was seen during the electrodeposition of Si_xGe_{1-x} films [36]. There the films consisted of different particles with variable sizes (around 2–20 nm) and due to the film growth the colour changed from red to blue-green. This change in colour was attributed to the absorbing of different wavelengths from the visible spectrum, because the particles

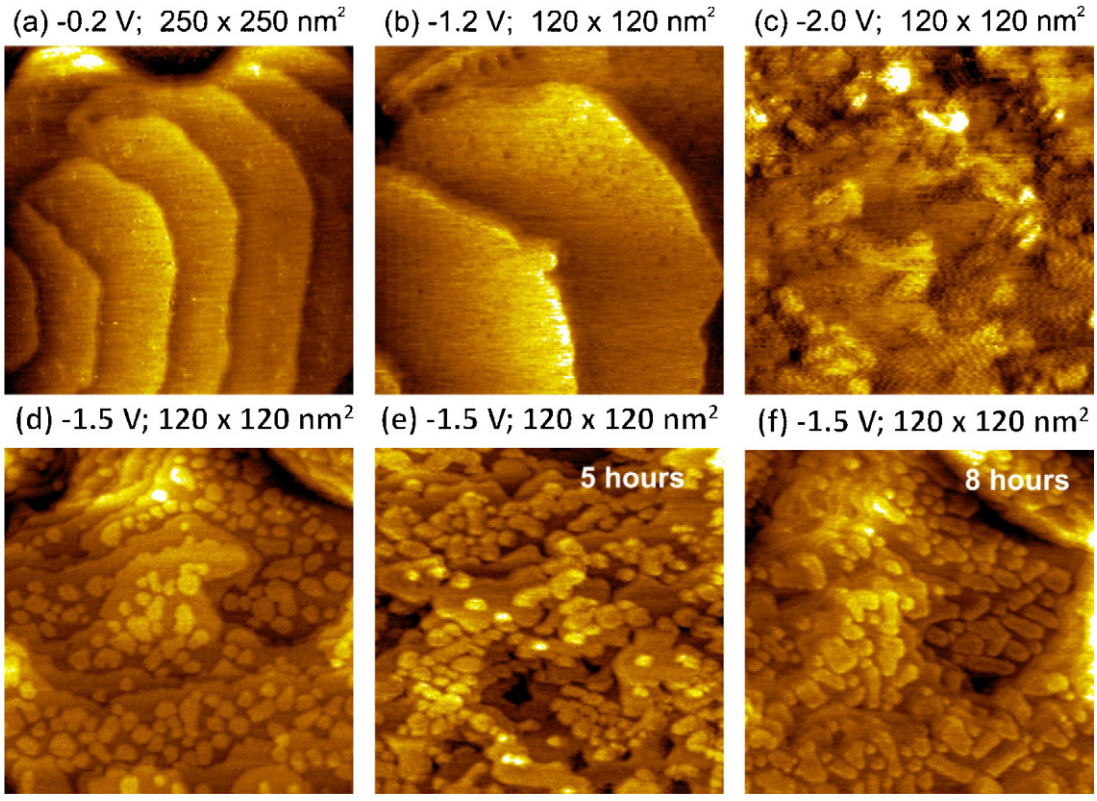

Fig. 3. *In situ* STM images of Au(1 1 1) surface in [EMIm]FAP at different electrode potentials.

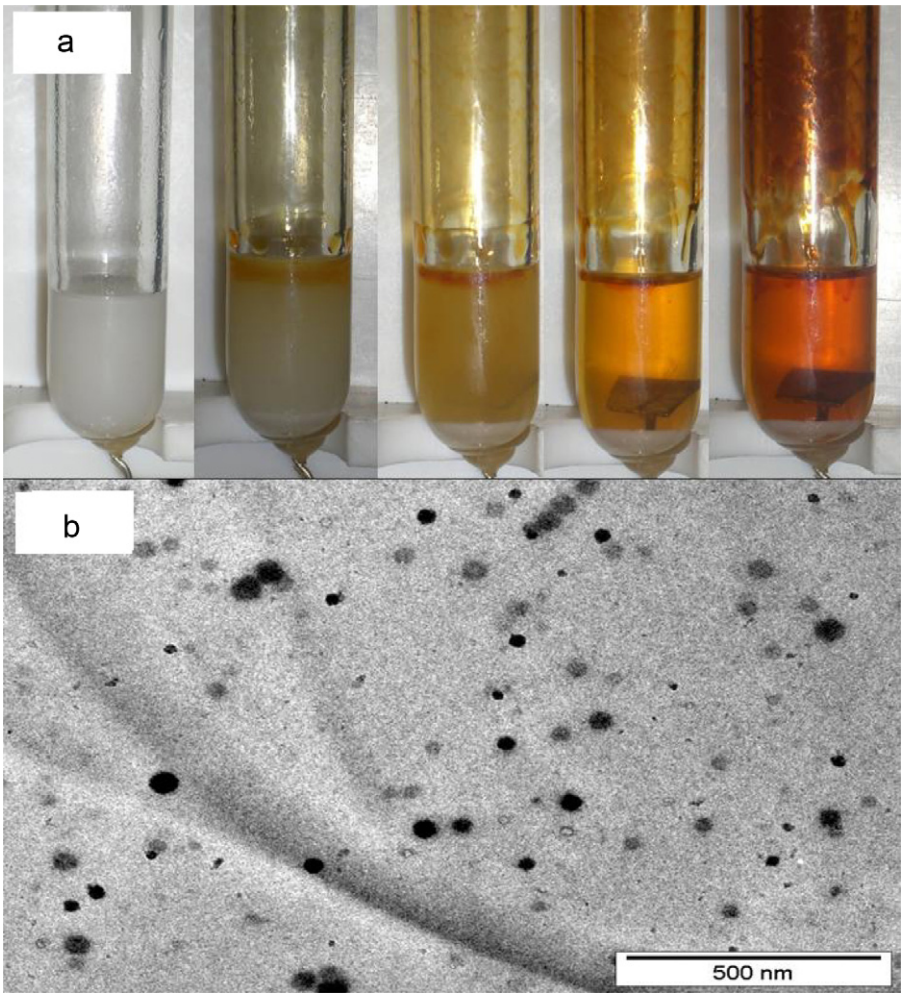

Fig. 4. (a) Plasma experiment for $GeCl_2$·dioxane-[EMIm]TFSA solution. (b) TEM image of Ge particles from $GeCl_2$·dioxane-[EMIm]TFSA.

exhibit different band gaps. We might explain the different colours observed here similarly as our free particles are in the same size regime. In future we will investigate this effect more in detail, in combination with chemical analysis of the particles. In general our particle sizes are in good agreement with germanium particles obtained by a chemical reaction between KGe and excess $GeCl_4$ in glyme solvents [37], or particles produced with non thermal plasma in a $GeCl_4$ argon gas flow [38]. We would like to mention that the plasma deposition of Si nanoparticles is more challenging. $SiCl_4$ and $SiBr_4$ are pumped off and from SiI_4 only non-stoichiometric SiI_x particles are obtained.

3.3. Electrodeposition of selenium under environmental conditions

Selenium is an important element for the production of semiconductor thin films of, e.g. InSe, CdSe or $CuInSe_2$ for advanced solar cells, IR detectors and solid-state laser applications [39]. Elemental selenium can exist in different phases: (1) amorphous phases (red, brown and black) which is rather an insulator, (2) crystalline phases, which include several solid allotrops, namely, the rhombohedral, α, β and γ monoclinic and trigonal (hexagonal) ones. Hexagonal Se is called the grey phase and it is the most stable one of all phases [40]. The electrodeposition of selenium from conventional aqueous electrolytes usually leads to the formation of insulating amorphous red selenium. Graham et al. [41] stated that amorphous Se layers with thicknesses up to 500 nm can be plated using acidic (pH 0.7–0.9) or slightly alkaline (pH 7.5–8.0) electrolytes in the temperature range 20–40 °C. However, they noticed that colloidal Se is produced near the cathode surface during plating. Such particles aggregate and increase in number and size with time causing defects in the deposited Se. Uzoh and Aksu got better results by addition of an anti-coagulation agent like 1,4-bis(3-aminopropyl) piperazine, during the plating process of Cu–Se [42]. Hippel et al. [43] successfully deposited the grey Se using an acidic electrolyte composed of saturated selenium dioxide in 9 M H_2SO_4 at a temperature of 100 °C. Accordingly, under such operating conditions (high acidity and high temperatures), electrodeposition of grey Se is difficult to apply to mass production. In this section we demonstrate that the deposition of crystalline Se can be realized at lower temperatures from air and water stable ionic liquids under environmental conditions. The cyclic voltammogram presented in Fig. 5 indicates that H_2SeO_3 in 1-butyl-1-methylpyrrolidinium trifluoromethylsulfonate containing 5 vol% of water is subject to 2 cathodic reduction processes (C_1–C_2) on gold at both studied temperatures (25 and 70 °C). Grey Se could only be deposited at 70 °C and it disappears on this potential scale at −2.5 V. A comparison with the results in a recent paper by Lai et al. is difficult as in ionic liquids different pathways might be possible. However, those authors interpreted the first process similar to our C_1 to the electroreduction of H_2SeO_3 to Se^0 through a four-electron step [44]. In their study the second process similar to our C_2 is due to a six-electron reduction of H_2SeO_3 to H_2Se. Both reduction products then undergo a conproportionation to elemental Se. The third peak

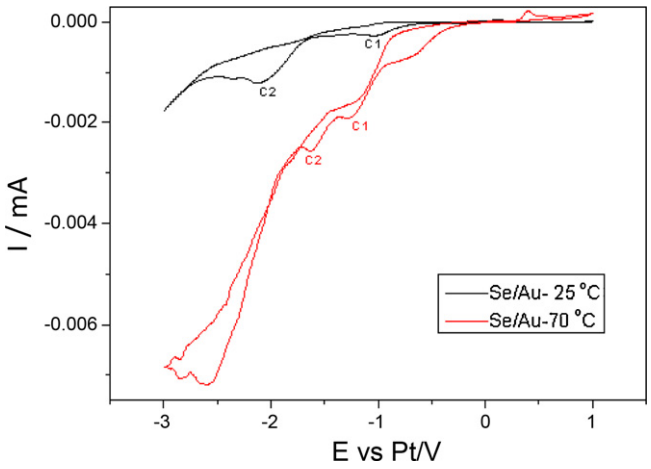

Fig. 5. CV of [Py1,4]TFO/water mixture containing H_2SeO_3 at different temperatures.

observed for the experiment at 70 °C might be due to the reduction of elemental Se to Se^{2-}.

The phase structure and chemical composition of the deposited Se films were characterized by X-ray diffraction and EDX, respectively (Fig. 6a and b). The comparison of the observed peaks with the standard data proves that the deposited selenium is a mixture of textured rhombohedral (JCPDS 32-0992) and hexagonal (JCPDS 42-1425) crystal phases. The EDX spectrum (Fig. 6b) indicated that the products were pure Se. The deposit is composed of regular micrometer-sized spheres with smooth surfaces and a diameter of less than 1 μm (inset of Fig. 6b).

3.4. Polystyrene opals and electrodeposited macroporous materials

3.4.1. Preparation of the polystyrene template

The preparation of opal structures made from polystyrene spheres, e.g. for the sake of 3-dimensional macroporous structures has been extensively described in literature [45,46]. In brief, monodispersed PS spheres are made by an emulsion polymerization method and by adjusting of the synthesis parameters different sphere sizes can be made. In many papers it is described that substrates are covered with PS spheres with, e.g. a vertical deposition method delivering well ordered hexagonal opal structures with thicknesses in the several micrometer regime. We tested several approaches from literature and had to make the inconvenient experience that we could hardly reproduce the literature results even if we followed the experimental procedures step by step. We concluded that each group might have an own set of parameters and that even slight variations in the experimental parameters can alter the quality of the polystyrene sphere opal structure. After these drawbacks we decided to employ an alcoholic route. Such a route was mentioned earlier in [47] but we found that the reproducibility is quite good and that our simple immersion method allows coating a variety of electrode materials with well arranged PS spheres in a short time. For this purpose PS spheres with diameters of 400, 581 nm or 600 nm (Duke Scientific) were centrifuged and subsequently resuspended in pure ethanol to give a 10 vol% PS suspension in ethanol. The substrates were cleaned directly before use as described in Section 2. For electrode preparation the substrates were dipped in the alcoholic polystyrene suspension at 38 °C and simply pulled out. It is advantageous to pull out the samples at an angle of about 45° between the sample and the surface normal of the suspension. This dipping process takes only a few seconds and the PS spheres self-assemble on the different materials mainly in an ordered hexagonal structure. We have to mention that the roughness of the surface plays a role and on flat surfaces, especially single crystals, the arrangement is best. We have also observed that before use as an electrode for metal deposition it is advantageous to slightly anneal the PS-covered electrode at 100 °C for 2 h. Fig. 7a shows a SEM image of an indium tin oxide (ITO) coated glass with PS spheres on top. The PS layer exhibits well ordered domains with a hexagonal structure separated by defects. Typical lateral dimensions of the single domains are up to 20 μm. If we coat polished Al with PS spheres we also get ordered domains with a hexagonal structure, but the lateral dimensions are lower, Fig. 7b. On Au(1 1 1), however, the lateral dimensions of such domains can be up to 50 μm with thicknesses of up to 20 μm. On rough metal substrates we hardly get ordered domains. Apart from the roughness also the purity of the substrate surface plays a role and we found that a thorough removal of organic contamination layers has a beneficial effect on the quality of the PS layers. When these substrates are used for electrodeposition the order of the final replica is strongly dependent on the material and the deposition parameters. A slow growth leads to well ordered structures whereas a (too) fast growth

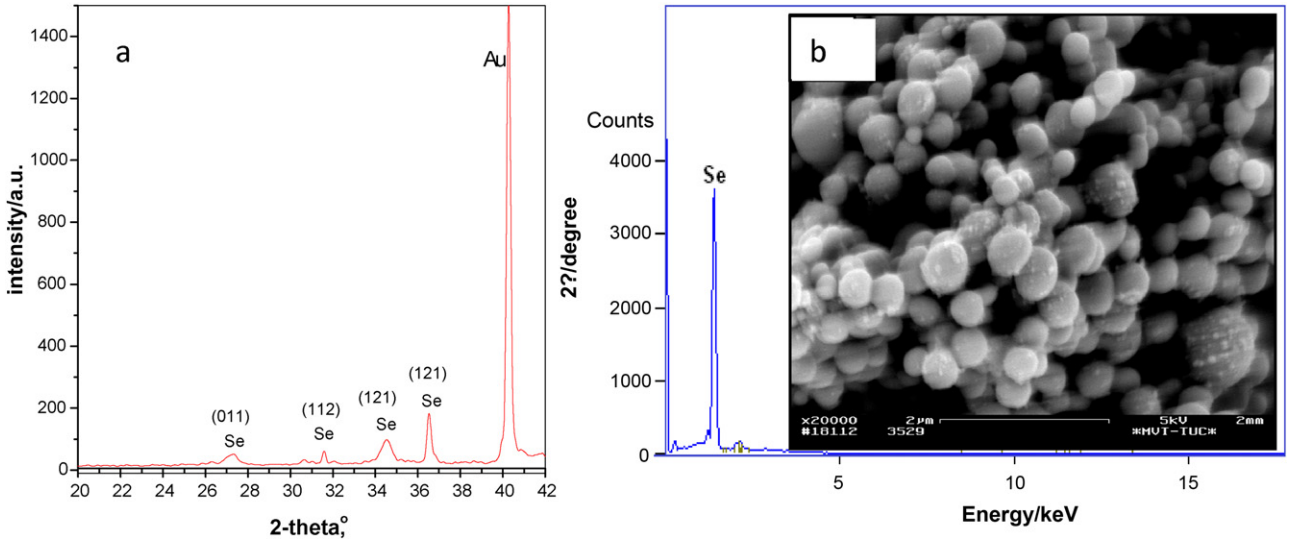

Fig. 6. X-ray diffraction (a) and SEM–EDX (b) analysis of Se film deposited on Au substrate from [Py1,4]TFO/water mixture at 70 °C.

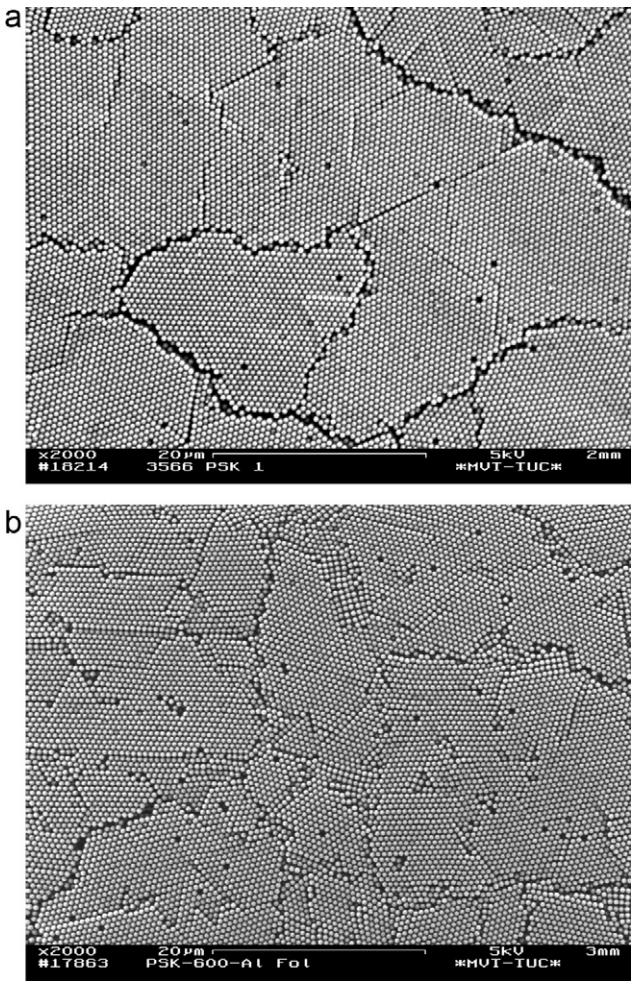

Fig. 7. (a) SEM image of 581 nm PS spheres on ITO. (b) SEM image of 600 nm PS spheres on aluminium foil.

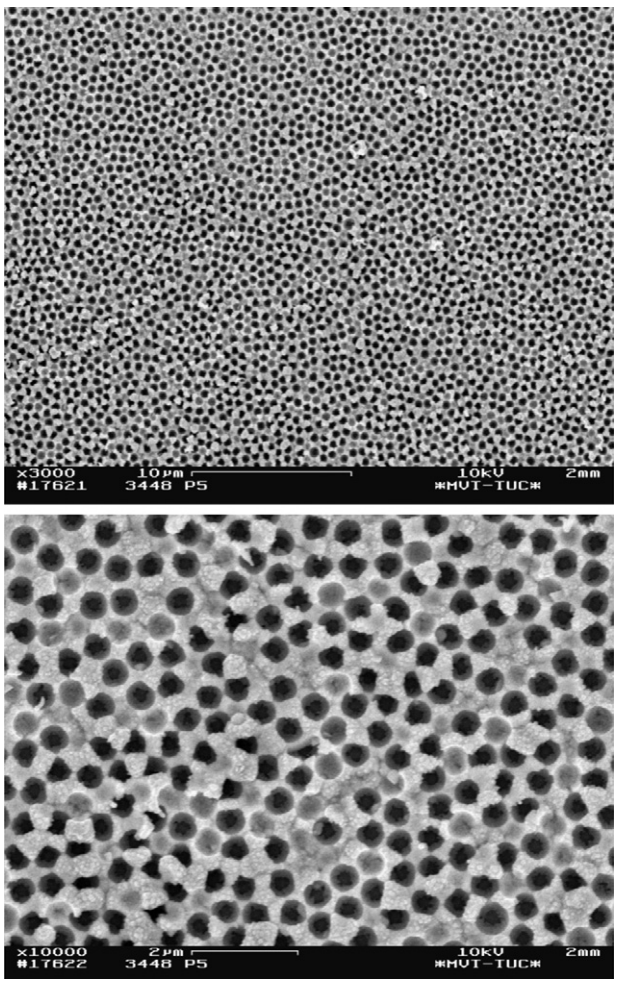

Fig. 8. SEM images with different magnifications of a macroporous Ag film electrodeposited on a PS-ITO substrate in the ionic liquid [EMIm]TfO containing 0.1 M Ag(TfO) at −0.6 V (vs. Ag) for 2 h.

rather leads to a not perfect structure even if the PS opal was quite good.

3.4.2. Macroporous silver

In this section we present our results on the electrodeposition of macroporous silver on ITO. The supplier gives a roughness of 100 nm, and this is a roughness where we observed that the PS spheres are not perfectly arranged. Nevertheless, as will be shown, substrates with a controlled pore size can be made and such materials are interesting as catalysts. The template-assisted electrodeposition of macroporous Ag films in two ionic liquids ([$Py_{1,4}$]TFSA and [$Py_{1,4}$]DCA) was recently reported by Chen et al. [48]. They introduced silver ions into the liquids by anodic dissolution of silver. For our experiments we employed the ionic liquid [EMIm]TfO with Ag(TfO) as a source of silver. Adherent macroporous silver films were fabricated via electrodeposition into the above described polystyrene (PS) templates self assembled onto indium tin oxide coated-glass substrates. A constant potential of −0.6 V (vs. Ag reference electrode) was applied for 2 h in the ionic liquid [EMIm]TfO containing 0.1 M Ag(TfO). After removing the PS template by dissolution in tetrahydrofuran (THF) an adherent macroporous Ag film was obtained. As shown in Fig. 8 the electrodeposited Ag film is highly porous giving rise to an increased catalytic activity. It is not perfectly hexagonally arranged which we mainly attribute to the roughness of the employed ITO electrode. A detailed study of the structural and optical properties of highly ordered 3DOM Ag films will be presented in a future paper.

3.4.3. Macroporous aluminium

Macroporous Al was obtained by the electrochemical deposition of Al from [EMIm]Cl:$AlCl_3$ (2:3 molar ratio) on a Au electrode covered by several layers of polystyrene spheres with a sphere diameter of 600 nm. The electrochemical behavior of this system

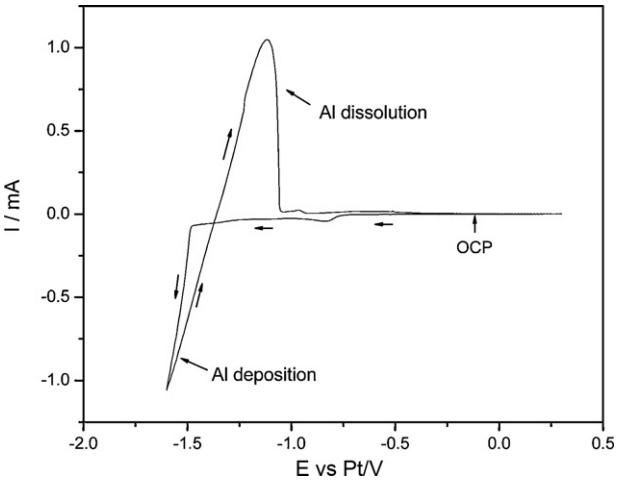

Fig. 9. CV of [EMIm]Cl/$AlCl_3$ (2:3 molar ratio) inside PS template (600 nm) on Au electrode. Scan rate = 10 mV/s, at 25 °C. OCP, open circuit potential.

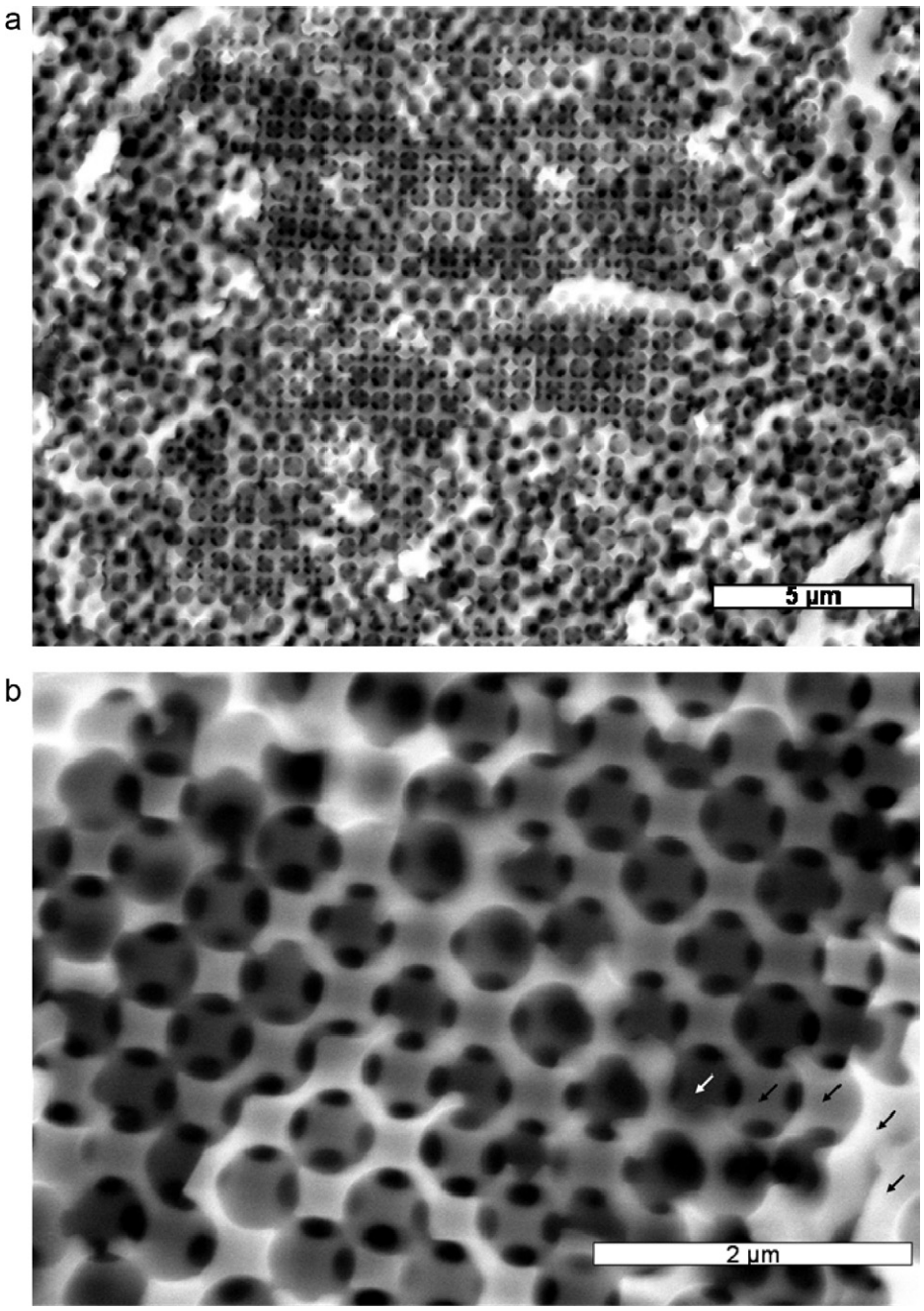

Fig. 10. SEM image of macroporous Al after removal of the PS template, obtained after applying a potential of −1.6 V for 5 min.

is presented in the cyclic voltammogram shown in Fig. 9: the CV exhibits – despite the PS spheres on top of the electrode – the typical behavior of Al deposition/stripping. For the deposition process, an electrode potential of −1.6 V on this potential scale was applied for 5 min. This short time was sufficient to fill the voids between the layers of the PS template. In this electrolyte the growth of Al can be quite fast and an over-filling of the template together with an alteration of the PS sphere packing can easily occur. Fig. 10 shows SEM images of the obtained macroporous Al after the removal of the template by THF. The macroporous structure can be clearly seen and the pores are of high density which ensures a very high surface area. Although we do not get a perfectly ordered porous structure there are short-range ordered areas in three dimensions. Such macroporous Al substrates are of interest as host materials for anodes in lithium secondary batteries and as a support for catalysts.

3.4.4. Macroporous silicon

To the best of our knowledge, no successful attempts have been reported on the synthesis of macroporous Si by an electrochemical pathway. From our experience, electrochemical synthesis of macroporous Si has proven to be much more difficult than that of macroporous Ge and Si_xGe_{1-x}. Herein, we report our first results in this field, which shows that macroporous Si can, in principle, be prepared by electrochemical deposition inside PS templates. Fig. 11 shows the cyclic voltammogram of 0.3 M $SiCl_4$ in $[Py_{1,4}]FAP$ on ITO-glass substrate covered with PS template (400 nm average sphere size): in the forward scan two small reduction peaks appear at potentials of −1.1 and −1.5 V vs. Pt quasi reference electrode which might be attributed to some solution reactions, e.g. the reduction of $SiCl_4$ to Si_xCl_{2x+2}. The third reduction peak at a potential of −1.3 V is

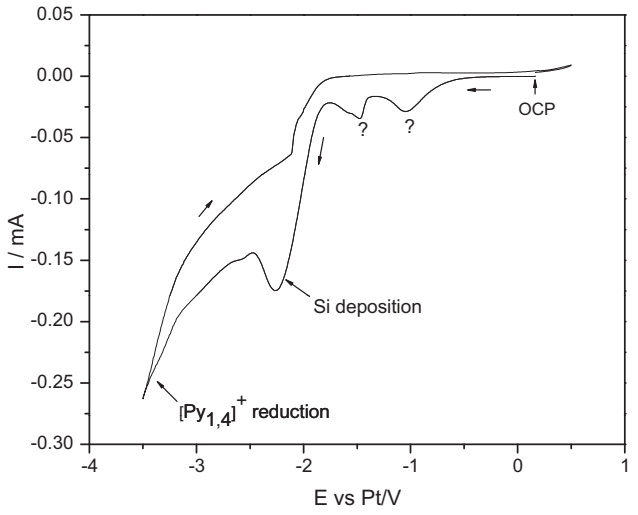

Fig. 11. CV of 0.3 M $SiCl_4$ in $[Py_{1,4}]$FAP inside PS template (400 nm) on ITO-glass electrode. Scan rate = 10 mV/s, at 25 °C. OCP, open circuit potential.

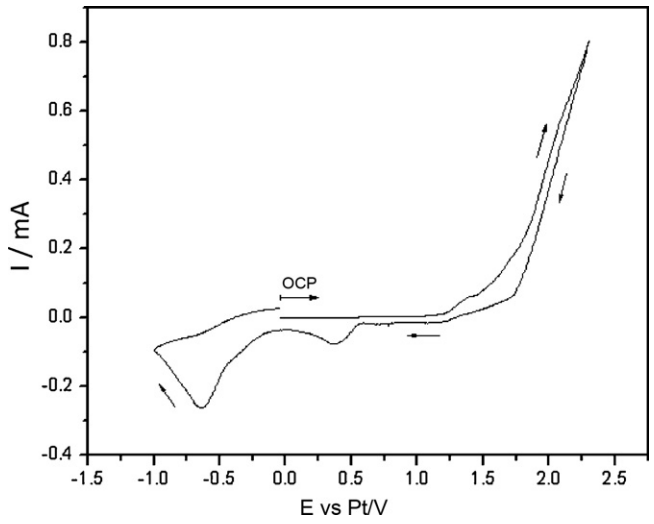

Fig. 13. Cyclic voltammogram of 0.1 mol/L EDOT in $[Py_{1,4}]$TFSA on Au substrate covered with a PS-template (600 nm average sphere size). Sweep rate 10 mV/s at 25 °C.

correlated with the bulk deposition of Si. No oxidation peaks were observed.

In order to deposit Si (inside the template) a potential of −2.4 V was applied for 1 h. The deposit was then removed from the glove box and washed with isopropanol to remove the electrolyte. The template was subsequently removed by THF. SEM images in Fig. 12 reveal the macroporous structure of Si. The high resolution SEM image in Fig. 12b shows that Si has a granular morphology with smallest grain size of less than 50 nm. Such a morphology was also obtained previously with Si deposition from an ionic liquid on bare Au electrodes [36]. We have to mention that the deposition of Si in these templates does not deliver perfectly arranged photonic crystals as reported for germanium in [20], rather individual 3DOM Si islands are obtained. We assume that during Si deposition in the PS opal structure a stress occurs which pushes away the PS spheres rather than filling the voids. This might be enhanced by the rapid oxidation of Si under environmental conditions. So far it is quite challenging to make photonic crystals of silicon.

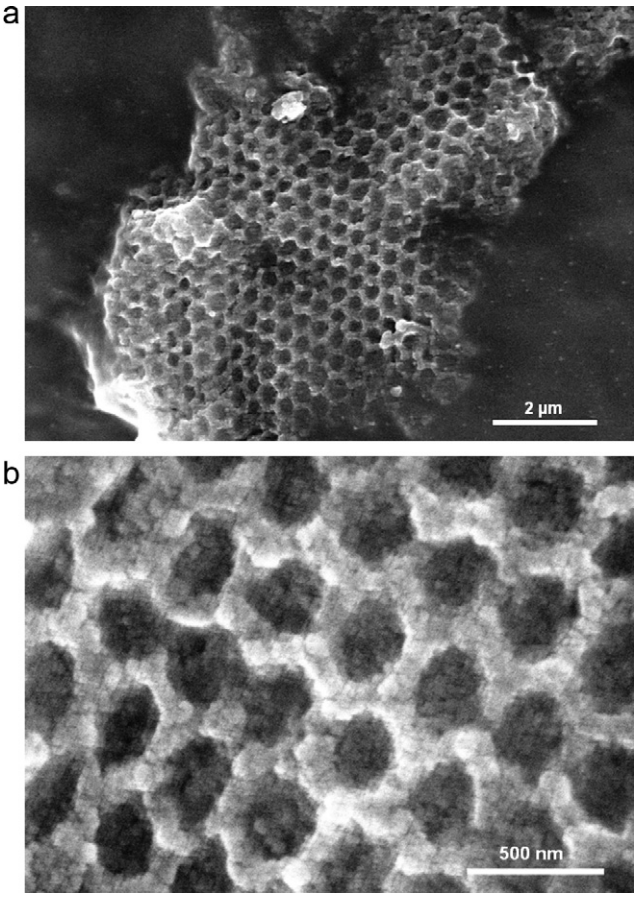

Fig. 12. SEM images of macroporous Si after removal of the PS template (400 nm), obtained after applying a potential of −2.4 V for 1 h.

3.4.5. Macroporous conducting polymers

Conducting polymers have received great attention as interesting materials for a variety of applications like in catalysis, in rechargeable batteries, as supports and as carriers in chromatography (ion-exchange resins) to mention a few [49]. They possess tunable redox properties and are environmentally stable. Poly(3,4-ethylenedioxythiophene) (PEDOT) and polyparaphenylene (PPP) are of particular interest: PEDOT possesses several useful properties such as optical transparency in its conducting state, high stability, moderate band gap and a low redox potential. PEDOT derivatives are now utilized in several industrial applications including as electrode materials in solid state capacitors, substrates for electroless metal deposition in printed circuit boards, as antistatic coatings for photographic films, as a replacement material for ITO in inorganic electroluminescent lamps, and as a hole-conducting material in organic/polymer-based light emitting diodes (OLEDs/PLEDs) [50–55]. In some of these applications a high surface area is needed and thus we attempted to make macroporous PEDOT by electrochemical means. Macroporous poly(3,4-ethylenedioxythiophene) (PEDOT) was successfully synthesized by electropolymerization of EDOT inside polystyrene (PS) templates in the ionic liquid 1-butyl-1-methylpyrrolidinium bis(trifluoromethylsulfonyl)amide ($[Py_{1,4}]$TFSA). Liquids with the TFSA anion belong to the best understood ones in the field of ionic liquids, and they can meanwhile be easily made in very high quality. Fig. 13 shows the cyclic voltammogram of 0.1 mol/L EDOT in $[Py_{1,4}]$TFSA on a polycrystalline Au substrate covered with a polystyrene (PS) template having an average sphere diameter of 600 nm (scan rate = 10 mV/s, at room temperature). The increasing anodic current at ~1.4 V vs. Pt quasi-reference electrode is corresponding to the bulk oxidative polymerization of EDOT monomer as a yellowish-brown deposit was observed which turns to dark

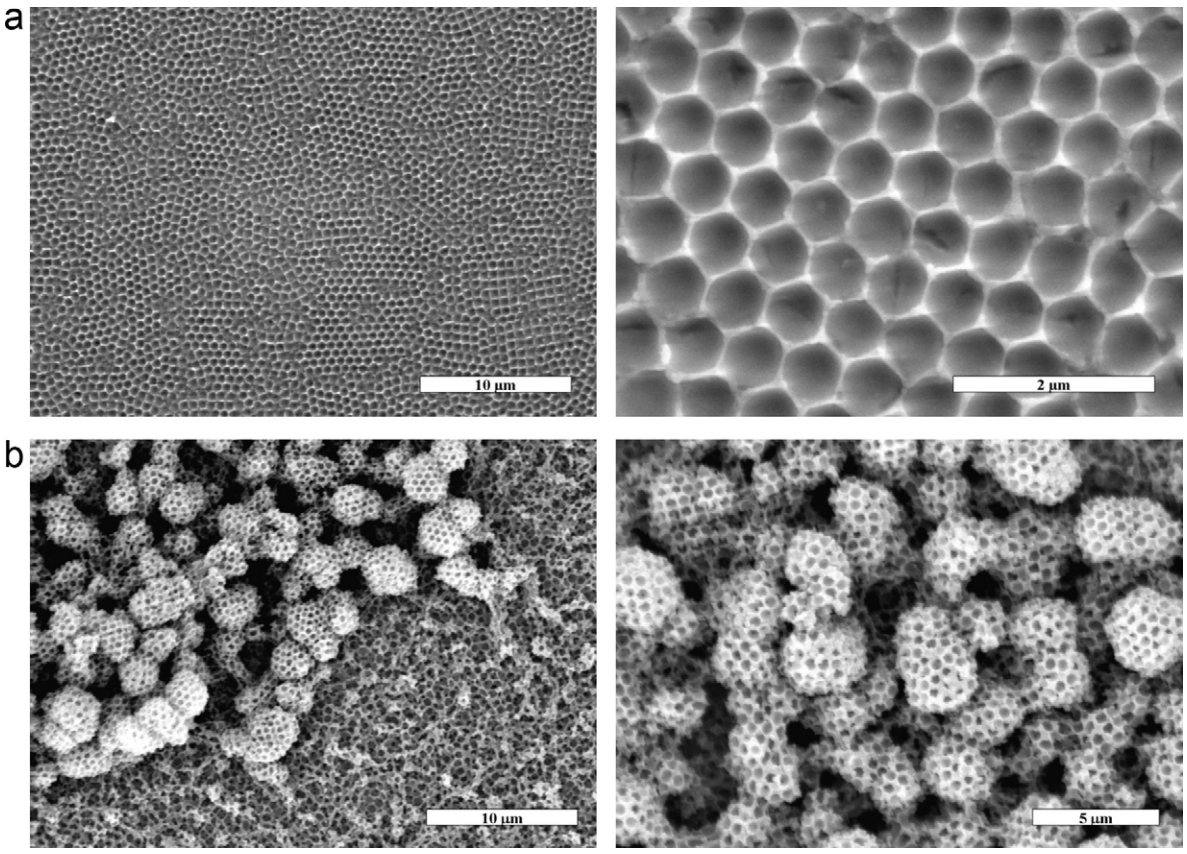

Fig. 14. SEM images of macroporous PEDOT after the removal of the PS template (600 nm). Applied potential = 1.7 V (a) for 5 min and (b) 1 h at 25 °C.

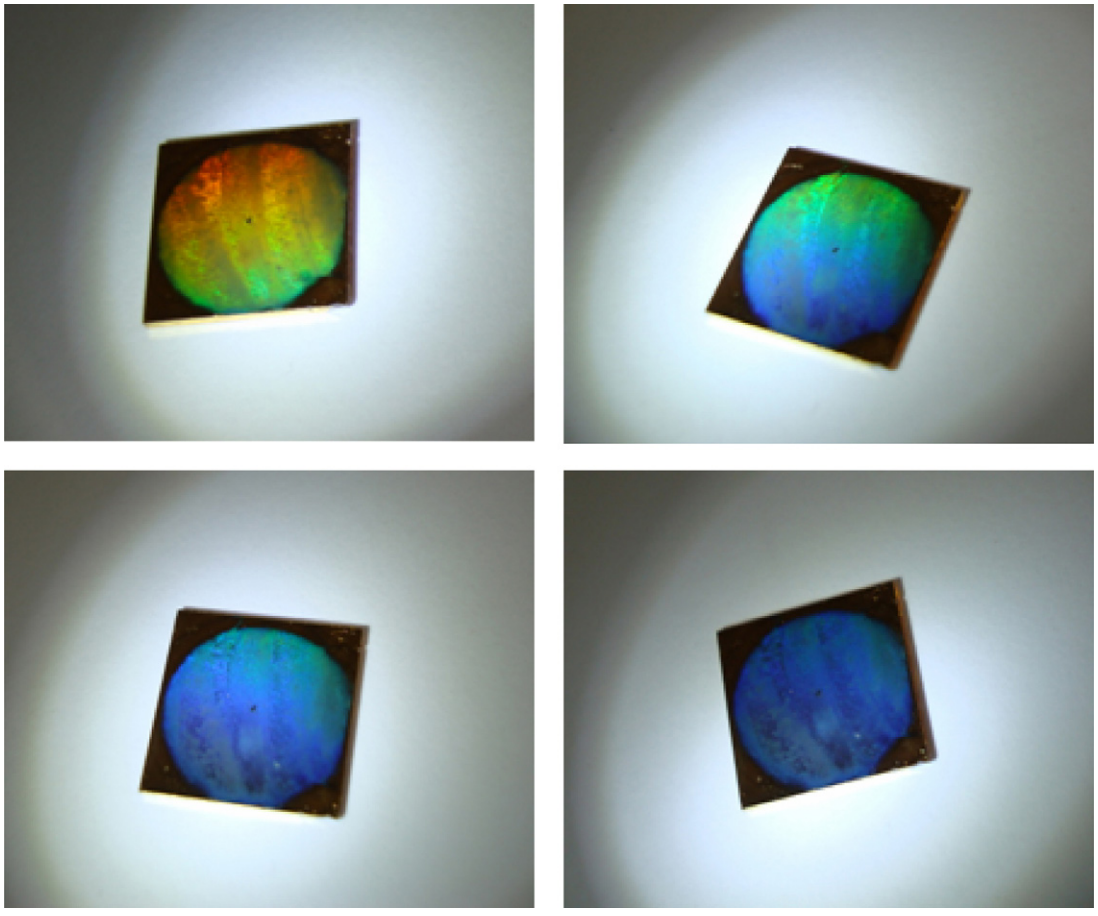

Fig. 15. Photographs of the macroporous PEDOT film (600 nm average pore size) on Au substrate after the removal of the PS template showing the colour change with slightly changing the angle of incident visible light.

blue with increasing the potential/thickness. In the back-scan, two reduction peaks were observed. As during oxidation there is both polymerization and doping the cathodic peaks represent the reduction of the formerly oxidized polymer. In order to obtain macroporous PEDOT, a potential of 1.7 V was applied (at room temperature) to the PS-covered Au working electrode for 1 h. The electrode was then removed from the glove box and rinsed with isopropanol to remove the electrolyte. The subsequent removal of the PS spheres by THF gave the expected macroporous structure of PEDOT. Fig. 14a shows SEM images of macroporous PEDOT deposits obtained after applying the desired potential for different periods of time. As can be seen, the macroporous structure of the polymer covers a large area which can be seen even on the 40 μm × 40 μm scale with individual domains having widths of about 5–7 μm. We also would like to mention that on the same substrate we observed structures like shown in Fig. 14b, which might be the result of inhomogenities in the electrical field during the electrodeposition process. A well ordered photonic crystal might require a geometrically optimized electrochemical cell. Fig. 15 finally shows photographs of the whole macroporous PEDOT deposit on Au substrate. The deposit gives rise to different colours when changing the angle of incident light owing to light reflections as has to be expected for a photonic crystal.

4. Conclusions

In the present paper we have summarized our recent results on the interfacial electrochemistry of and electrodeposition from ionic liquids. We could show that the interface Au(1 1 1)/ionic liquid is a good candidate for surprises. With $[Py_{1,4}]$FAP having all impurity below 10 ppm we see a restructuring of the surface which is different from what we observed in [EMIm]FAP. In a certain potential regime we see the famous herringbone superstructure of Au(1 1 1) which we do not see in [EMIm]FAP of the same quality. Furthermore the interface Au(1 1 1)/[EMIm]FAP reveals slow processes and there are hints for the adsorption of the cation. The plasmaelectrochemical experiment has shown that germanium nanoparticles can be made and there are hints for a size dependent colour. Selenium can be electrodeposited from ionic liquids under environmental conditions at varying temperatures which might have some potential in an industrial process for the making of CIS solar cells. As will be shown in a later paper homogeneous layers of different phases are feasible. Our studies on macroporous materials have shown that with an alcoholic suspension of polystyrene spheres a variety of substrates can be easily covered. Especially for the sake of macroporous electrode materials, e.g. for batteries or materials in secondary batteries, our process is fast and coating only takes a few seconds. Macroporous Ag, Al, Si and PEDOT can be made. Even with almost perfectly arranged PS spheres also the electrochemical parameters during deposition play a great role. A too fast deposition rate can corrupt the quality of the PS opal, and the deposition of 3DOM Si is remarkably difficult.

Acknowledgments

This work was financially supported by the Deutsche Forschungsgemeinschaft (DFG), the Federal Ministry of Education and Research (BMBF), the Alexander von Humboldt Association with a grant to Dr. Aal and EFZN Goslar, Germany (www.efzn.de).

References

[1] Y. NuLi, J. Yang, P. Wang, Appl. Surf. Sci. 252 (2006) 8086.
[2] Z. Feng, Y. NuLi, J. Wang, J. Yang, J. Electrochem. Soc. 135 (2006) C689.
[3] I. Mukhopadhyay, C.L. Aravinda, D. Borissov, W. Freyland, Electrochim. Acta 50 (2005) 1275.
[4] G.T. Cheek, W.E. O'Grady, S. Zein El Abedin, E.M. Moustafa, F. Endres, J. Electrochem. Soc. 155 (2008) D91.
[5] F. Endres, S. Zein El Abedin, A.Y. Saad, E.M. Moustafa, N. Borisenko, W.E. Price, G.G. Wallace, D.R. MacFarlane, P.J. Newman, A. Bund, Phys. Chem. Chem. Phys. 10 (2008) 2189.
[6] N. Borisenko, A. Ispas, E. Zschippang, Q. Liu, S. Zein El Abedin, A. Bund, F. Endres, Electrochim. Acta 54 (2009) 1519.
[7] F. Endres, O. Höfft, N. Borisenko, L.H.S. Gasparotto, A. Prowald, R. Al-Salman, T. Carstens, R. Atkin, A. Bound, S. Zein El Abedin, Phys. Chem. Chem. Phys. 12 (2010) 1724.
[8] M.V. Fedorov, A.A. Kornyshev, J. Phys. Chem. B 112 (2008) 11868.
[9] R. Atkin, G.G. Warr, J. Phys. Chem. C 111 (2007) 5162.
[10] C.A. Zell, W. Freyland, Langmuir 19 (2003) 7445.
[11] O. Mann, G.-B. Pan, W. Freyland, Electrochim. Acta 54 (2009) 2487.
[12] Y.-Z. Su, Y.-C. Fu, J.-W. Yan, Z.-B. Chen, B.-W. Mao, Angew. Chem. Int. Ed. 48 (2009) 5148.
[13] B.R. Clare, P.M. Bayley, A.S. Best, M. Forsyth, D.R. MacFarlane, Chem. Commun. (2008) 2689.
[14] S.A. Meiss, M. Rohnke, L. Kienle, S. Zein El Abedin, F. Endres, J. Janek, ChemPhysChem 8 (2007) 50.
[15] Y.B. Xie, C.L. Liu, Plasma Process. Polym. 5 (2008) 239.
[16] T. Kaneko, K. Baba, T. Harada, R. Hatakeyama, Plasma Process. Polym. 6 (2009) 713.
[17] S. Zein El Abedin, A.Y. Saad, H.K. Farag, N. Borisenko, Q.X. Liu, F. Endres, Electrochim. Acta 52 (2007) 2746.
[18] T.A. Sorenson, T.E. Lister, B.M. Huang, J.L. Stickney, J. Electrochem. Soc. 146 (1999) 1019.
[19] M. Alanyalioglu, U. Demir, C. Shannon, J. Electroanal. Chem. 561 (2004) 21.
[20] X. Meng, R. Al-Salman, J. Zhao, N. Borissenko, Y. Li, F. Endres, Angew. Chem. Int. Ed. 48 (2009) 2703.
[21] R. Al-Salman, X. Meng, J. Zhao, Y. Li, U. Kynast, M.M. Lezhnina, F. Endres, Pure Appl. Chem. 82 (2010) 1673.
[22] L.H.S. Gasparotto, A. Prowald, N. Boresinko, S. Zein El Abedin, F. Endres, J. Power Sources 196 (2011) 2879.
[23] M. Brettholle, O. Höfft, L. Klarhöfer, S. Mathes, W. Maus-Friedrichs, S. Zein El Abedin, S. Krischok, J. Janek, F. Endres, Phys. Chem. Chem. Phys. 12 (2010) 1750.
[24] J.V. Barth, H. Brune, G. Ertl, R.J. Behm, Phys. Rev. B 42 (1990) 9307.
[25] Ch. Wöll, S. Chiang, R.J. Wilson, P.H. Lippel, Phys. Rev. B 39 (1989) 7988.
[26] V. Repain, J.M. Berroir, S. Rousset, J. Lecoeur, Appl. Surf. Sci. 162–163 (2000) 30.
[27] H. Oka, K. Sueoka, Jpn. J. Appl. Phys. 44 (2005) 5430.
[28] Y. Hasegawa, Ph. Avouris, Science 258 (1992) 1763.
[29] D.M. Kolb, Prog. Surf. Sci. 51 (1996) 109.
[30] J. Schneider, D.M. Kolb, Surf. Sci. 193 (1988) 579.
[31] N.J. Tao, S.M. Lindsay, Surf. Sci. Lett. 274 (1992) L546.
[32] D.M. Kolb, Andew. Chem. Int. Ed. 40 (2001) 1162.
[33] D.M. Kolb, J. Schneider, Electrochim. Acta 31 (1986) 929.
[34] N. Borisenko, S. Zein El Abedin, F. Endres, J. Phys. Chem. B 110 (2006) 6250.
[35] R. Atkin, S. Zein El Abedin, L.H.S. Gasparotta, R. Hayes, N. Borisenko, F. Endres, J. Phys. Chem. C 113 (2009) 13266.
[36] R. Al-Salman, S. Zein El Abedin, F. Endres, Phys. Chem. Chem. Phys. 10 (2008) 4650.
[37] B.R. Taylor, S.M. Kauzlarich, G.R. Delgado, H.W.H. Lee, Chem. Mater. 11 (1999) 2493.
[38] R. Gresback, Z. Holman, U. Kortshagen, Appl. Phys. Lett. 91 (2007) 093119.
[39] H.W. Schock, Appl. Surf. Sci. 92 (1996) 606.
[40] Y. Miyamoto, Jpn. J. Appl. Phys. 19 (1980) 1813.
[41] A.K. Graham, H.L. Pinkerton, H.J. Boyd, J. Electrochem. Soc. 106 (1959) 657.
[42] C. Uzoh, S. Aksu, US patent 12/642691, 2010.
[43] A. Hippel, US Patent no 2,649,409, 1953.
[44] Y. Lai, F. Liu, J. Li, Z. Zhang, Y. Liu, J. Electroanal. Chem. 639 (2010) 187.
[45] J.H. Kim, M. Chainey, M.S. El-Aasser, J.W. Vanderhoff, J. Polym. Sci. Part A 27 (1989) 3187.
[46] M.A. McLaclan, N.P. Johnson, R.M. De La Rue, D.W. McComb, J. Mater. Chem. 14 (2004) 144.
[47] Z. Zhou, X.C. Zhao, Langmuir 20 (2004) 1524.
[48] M.-C. Tsai, D.-X. Zhuang, P.-Y. Chen, Electrochim. Acta 55 (2010) 1019.
[49] F. Svec, J.M.J. Frechet, Science 273 (1996) 205.
[50] L. Groenendaal, F. Jonas, D. Freitag, H. Pielartzik, J.R. Reynolds, Adv. Mater. 12 (2000) 481.
[51] F. Jonas, L. Schrader, Synth. Met. 41–43 (1991) 831.
[52] G. Heywang, F. Jonas, Adv. Mater. 4 (1992) 116.
[53] I. Winter, C. Reece, J. Hormes, G. Heywang, F. Jonas, Chem. Phys. 194 (1995) 207.
[54] M. Dietrich, J. Heinze, G. Heywang, F. Jonas, J. Electroanal. Chem. 369 (1994) 87.
[55] http://www.agfa.com/sfc/polymer.